Kinetics of long-wavelength infrared stimulation of donor-acceptor pair luminescence in ZnS†

J. W. Allen*
Lincoln Laboratory, Massachusetts Institute of Technology, Lexington, Massachusetts 02173
(Received 3 August 1973)

This paper describes some experimental kinetic and spectroscopic studies in ZnS of photoluminescence stimulated by 8.8 and 10.6-μm infrared radiation. The results of a theoretical model of the stimulation process are also presented. The model is based on the donor-acceptor pair-luminescence theory and the assumption that the infrared radiation induces donor-level–to–conduction-band transitions. The model results are in good qualitative agreement, and fair quantitative agreement with the experimental observations.

I. INTRODUCTION

A. Perspective

It has been known for at least 25 years that short-wavelength infrared radiation ($\lambda < 3$ μm) can quench or stimulate the photoluminescence of many ZnS phosphors.[1] A review of this work up to 1965 has been given by Mason.[2] However, the realization that longer-wavelength radiation often has similar effects is much more recent. In a series of papers[3–6] beginning in 1966, Baur, Riehl, and co-workers have reported and discussed observations of stimulation of luminescence in ZnS with infrared radiation in the wavelength range 3–25 μm. Their experiments were carried out in the phosphor afterglow period (after the cessation of photoexcitation) and they found that the size of the stimulation diminished with the amount of time between cessation of photoexcitation and application of infrared radiation. By combining thermal-glow-curve measurements with infrared stimulation experiments, they determined that longer-wavelength stimulation involves the release of electrons from very shallow electron traps. They also measured the infrared-wavelength dependence, the temperature dependence, and the spectral distribution of the stimulated luminescence. Finally, they reported that the rise time of the stimulated luminescence was less than 1 msec.

This paper describes some experimental kinetic and spectroscopic studies in ZnS of luminescence stimulated by longer-wavelength infrared, and also presents the results of a theoretical kinetic model of the stimulation process. The samples used in this study are not particularly well characterized in terms of impurity content, and so this paper focuses on several aspects of the infrared-stimulation phenomenon that are not sample dependent. Most of the experiments were carried out with steady photoexcitation, in contrast to the afterglow work of Baur *et al.* The infrared-radiation-intensity dependence, the temperature dependence, and spectral distribution of the stimulated luminescence have been measured. In addition the stimulated-luminescence waveforms produced by step function and repetitively pulsed infrared radiation have been determined. A measurement of infrared absorption is motivated and described in Sec. I B. Efforts to test for photoconductivity due to applied infrared radiation failed, as mentioned in Sec. II A. The experimental results are largely in accord with or complementary to those of Baur *et al.*, with the principal important exception that the stimulated luminescence was found to be shifted slightly to higher energies (blue shift) relative to that produced by steady photoexcitation. Baur *et al.* have reported that the two spectra are identical. The theoretical model is based on a recent reformulation of the kinetics of donor-acceptor pair luminescence by Dohler.[7] It suffices for the moment to comment that the model differs from that proposed by Baur *et al.* The differences are discussed in Sec. V.

B. Qualitative presentation of model

The basic stimulation phenomenon is that at sufficiently low temperatures the sudden application of infrared radiation to a steadily photoexcited phosphor produces a transient burst of additional luminescence. After the burst, the luminescence intensity returns nearly to its original value, but may be somewhat higher or lower. The experiment can also be performed after photoexcitation has ended, in the afterglow, and in this case the sudden application of infrared radiation also produces a transient burst and shortens the time of the afterglow. Qualitatively, two important experimental results of the present work are that the luminescence burst is spectrally very similar to that produced during steady photoexcitation, but slightly shifted to higher energies, and that the ratio of the transient-peak intensity to the steady background intensity decreases as the photoexcitation intensity increases.

Because the spectral character of the transient burst of luminescence is nearly the same as that of the luminescence due to steady photoexcitation, it is convenient, in seeking an understanding of the over-all phenomenon, to consider separately the luminescence mechanism and the stimulation mechanism. Visible luminescence in ZnS occurs because of the intentional or accidental presence of impurities in the crystal. The characteristics of the luminescence depend greatly on what the impurities are. For the materials used in the present study, there is a considerable body of evidence[8-11] that the luminescence is fairly well described by the donor-acceptor pair model, in which electrons make direct transitions from shallow-donor (electron-trap) states to deep-acceptor (hole-trap) states. The transition probability W for this process depends on the separation r of the donor and acceptor, and the dependence is often taken to be $W(r) = W_0 e^{-r/r_0}$, where r_0 is half the hydrogenic radius a_0 of the donor ground state. The energy E of the emitted photon also depends on r because of the Coulombic attraction $-e^2/\kappa r$ in the final state between the empty donor and the occupied acceptor (κ is the static dielectric constant). E is generally taken to be $E = E_G - E_D - E_A + e^2/\kappa r$, where E_G is the energy gap, E_D is the donor binding energy, and E_A is the acceptor binding energy. This type of luminescence is characterized by long decay times after cessation of photoexcitation at low temperatures due to trapped hole-electron pairs with large r and small W; by a red shift during decay because the small-r large-W large-E pairs decay first; by a blue shift with increased intensity steady photoexcitation because the large-r, small-W small-E pairs are easily saturated. These characteristics were observed for the luminescence of the samples used in the experiments reported here.

It is generally agreed[2-6] that the stimulation involves energy storage by photoexcited electrons and holes occupying trap states, and that the infrared radiation acts to release the stored energy by freeing the trapped holes or electrons, which then recombine radiatively. In the model assumed in the present work, energy storage is accomplished by photoexcited holes and electrons occupying large-r small-W donor-acceptor trap pairs. Dohler[7] has shown that for steady photoexcitation, these large-r traps will be nearly always full, while the small-r large-W traps will be nearly always empty. Most of the luminescence is due to the flow of traffic through the small-r large-W traps. The long-wavelength infrared is assumed to lift electrons from the filled large-r traps into the conduction band. They are subsequently retrapped with equal probability into any unfilled trap. Thus there is a statistical preference for retrapping into the (nearly always empty) small-r traps, from which radiative recombination quickly occurs with the hole on the nearby acceptor. The increased recombination traffic through the small-r traps causes an increase in the luminescence, which is spectrally blue-shifted relative to the luminescence produced by steady photoexcitation, as is experimentally observed. As the photoexcitation intensity increases, the steady background luminescence increases more than the stimulated luminescence, as observed experimentally, because the large-r energy storage traps tend to saturate. The points of the two preceding sentences are in close analogy with the last two characteristics of donor-acceptor pair luminescence mentioned in the preceding paragraph. To the extent that photoexcitation does not deplete the ground-state population, the rate of creation of hole-electron pairs is a constant fixed by the photoexcitation intensity. Also, if the only hole-electron recombination mechanism is radiative, the rate of photon production in steady state must equal the hole-electron pair generation rate whether or not there is infrared radiation present. Thus for photoexcitation intensities not too high, and if nonradiative recombination processes are small, the luminescence-intensity change induced by the infrared radiation must be transient, as observed.

In this model, the infrared radiation is absorbed by photoexcited electrons trapped at donors. In the absence of photoexcitation, the donors are not occupied and infrared absorption should not occur. For ZnS: Cu, Al, it has been reported[12] that photoexcitation induces infrared absorption in the 3–14-μm range, and that the decay of the absorption after cessation of photoexcitation is related to the decay of luminescence.[8] The absorption was interpreted[12] as donor-level–to–conduction-band transitions of electrons that had been photoexcited and trapped at the donors, as in the model of this paper. This model also implies that the infrared transmission should increase during the time infrared radiation is applied, because trapped electrons freed by the infrared radiation are retrapped at sites where radiative recombination is likely, thus decreasing the number of trapped electrons. Infrared transmission measurements made in the present study showed a large decrease with photoexcitation and an increase with application of infrared radiation.

C. Organization of paper

The remainder of this paper is organized as follows. Section II describes the experimental kinetic and spectroscopic data that have been obtained. In Sec. III approximate rate equations describing the detailed kinetics of the preceding model are developed. A variety of numerical solutions

of the equations that illustrate the detailed behavior of the model are presented in Sec. IV. In Sec. V the dependence of the model's behavior on various aspects of its parameters is explored, and the model results are compared with the experimental ones. Section VI discusses the relation of the present work to previous work, and makes a general appraisal. The method of solution of the equations is described briefly in Appendix A, and Appendix B discusses a more rigorous set of equations than the ones actually used.

II. EXPERIMENTAL RESULTS

A. Methods

Two experimental arrangements were employed. The first was designed to provide maximum protection of the sample from inadvertent exposure to background infrared radiation. Such protection was found to be quite important in obtaining a large stimulation effect.[5] The infrared source was an 8.8-μm laser diode mounted with the sample in a copper can. The copper can was provided with a single window that transmitted visible and ultraviolet radiation and blocked infrared radiation for wavelengths greater than 1 μm. The can, with its window, was placed in a liquid-helium Dewar. Thus the environment of the sample was at 4.2 K and the only significant source of infrared radiation was the diode. Since the diode response time is very fast (less than a microsecond), it was well suited as a source for kinetic studies of the stimulation process. Ultraviolet light was obtained by passing the light from a xenon discharge lamp through a $\frac{1}{2}$-m grating monochromator, or from a nitrogen-laser-pumped tunable dye laser. The xenon-lamp intensity was varied with neutral-density filters. The sample luminescence was collected and analyzed with a 1-m grating monochromator equipped with a cooled S-20 photomultiplier The output of the photomultiplier was displayed on an oscilloscope and photographed, or was analyzed with a boxcar integrator, depending on whether the diode was turned on abruptly and kept on, or pulsed repetitively.

The second experimental arrangement differed from the first in that the infrared source was a CO_2 laser operating in several modes around 10.6 μm. This provided much-higher infrared intensity and also permitted the sample temperature to be varied, which was not possible in the first arrangement because the laser diode had to be operated at temperatures near 4.2 K. Repetitive infrared pulses were obtained by chopping the laser beam at various rates and duty cycles. Intensity was varied by passing the laser beam through a variable-pressure gas-absorption cell. The sample was mounted in a copper can as described above, but having additionally two low-temperature narrow-bandpass 10.6-μm filter windows mounted 180° apart. Use of the filters permitted exposure of the sample to the laser beam with only a narrow spectral band of background blackbody radiation being able to reach the sample. Use of two windows allowed monitoring the infrared radiation transmitted through the sample with a Ge:Cu detector. The copper can was mounted in a variable-temperature Dewar equipped with the necessary windows to pass the infrared-laser beam, the ultraviolet pump light, and the luminescence in or out.

In those experiments where both the infrared radiation and the ultraviolet photoexcitation were applied as repetitive pulses, the two sources were triggered from a common reference to ensure maintenance of relative phase, and the relative phase was controlled by passing the reference for one of the sources through a variable delay line. For the xenon lamp and the CO_2 laser, this entailed the use of phase sensitive choppers.

An attempt to search for infrared stimulated photoconductivity failed, owing to the inability to make electrical contacts that were operable at the low temperatures where infrared stimulation of luminescence is observed. This problem has been reported previously.[11]

B. Samples

Experiments were conducted primarily on two crystalline ZnS samples. One was obtained from the Eagle Picher Company doped nominally with copper and aluminum. Mass spectrographic analysis revealed 400-ppm Al, 40-ppm Cu, and the presence of a number of other impurities, including O, N, B, Cl, and K, in concentrations similar to that of the Cu. The second sample was a nominally undoped ZnS crystal, although analysis again revealed a number of impurities in the 10-ppm range. The first sample displayed primarily the characteristic copper green luminescence, and also a very weak blue luminescence, which was not infrared stimulable. The second sample displayed self-activated blue luminescence that was infrared stimulable. The data shown in this paper are all for the ZnS:Cu, Al sample, because the data from both samples were substantially the same, except for the color of luminescence.

C. Time dependence of stimulated luminescence and infrared transmission

Figure 1 shows a typical oscilloscope trace obtained by exposing a sample to steady photoexcitation and abruptly turning on the laser diode. There is a rise in the luminescence intensity, and a peak is reached in about 5 msec. The luminescence then decays much more slowly, reaching its original level after about 0.5 sec. The decay is found

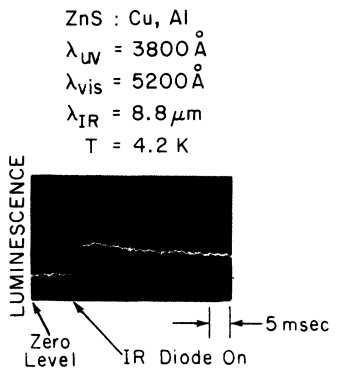

FIG. 1. Photograph of oscilloscope trace of photomultiplier current, showing transient change in steady photoluminescence due to step-function infrared radiation.

to be nonexponential and does not fit a power law. The size of the transient peak increases with the time of prior exposure to photoexcitation for exposure times up to about 5–10 sec, after which there is no further increase. When the diode is turned off, there is an abrupt decrease in the luminescence level, followed by a slow return to the original level in about 5–10 sec.

Figure 2 shows the stimulated-luminescence waveform resulting from photoexciting a sample steadily and pulsing the infrared diode repetitively. The waveform is obtained by scanning the gate of the boxcar integrator. It can be seen that the effect of turning off the infrared well before the completion of the decay seen in Fig. 1 is to return the luminescence to its original level in a time only slightly longer than the rise time to the peak. The height of the transient peak obtained by repetitively pulsing the diode is always less than that obtained by exposing the sample to photoexcitation for at least 5–10 sec and then abruptly turning on the diode. Also the transient peak decreases as the pulse repetition rate increases.

Figure 3 shows the luminescence waveform obtained with chopped photoexcitation (50% duty cycle) and chopped infrared radiation (4% duty cycle). The photoluminescence rise and fall times are both longer than the on and off periods of the photoexcitation. The infrared-radiation pulse is shown occurring during the photoluminescence decay as an example of stimulation in the afterglow region. The height of the stimulated-luminescence pulse is only slightly larger when the infrared pulse occurs during an "on" period in the photoexcitation repetition cycle. This implies that the stored charge responds even more slowly to the abrupt switching of the photoexcitation than does the luminescence.

The time dependence of the infrared transmission was measured for the case of steady photoexcitation and the sudden application of steady infrared radiation. This is somewhat difficult for very short times, since no signal can be measured at all until the infrared is turned on. It was found that over the period during which the stimulated luminescence achieves its peak there is essentially no change in the infrared transmission, but that an increase can be detected after about 100 msec, and this change continues for about 2 or 3 sec until a new, final, higher transmission value is reached. The extent to which this behavior is in accord with the model of Sec. I is discussed in Sec. IV.

D. Luminescence, stimulated luminescence, and photoexcitation spectra

Figure 4 shows time-resolved luminescence spectra obtained from the ZnS: Cu, Al sample un-

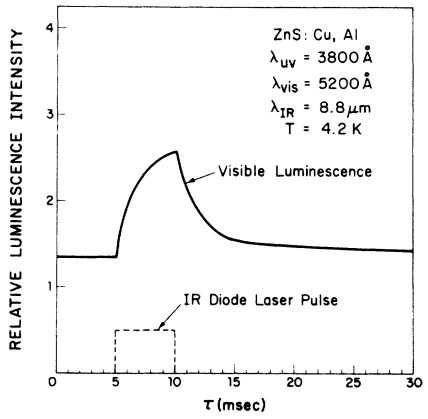

FIG. 2. Luminescence waveform obtained with steady photoexcitation and repetitively pulsed infrared radiation.

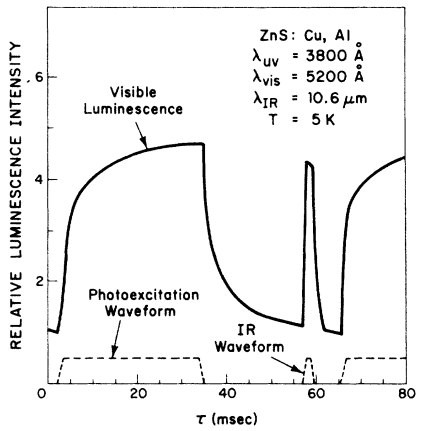

FIG. 3. Luminescence waveform obtained with chopped photoexcitation and repetitively pulsed infrared radiation.

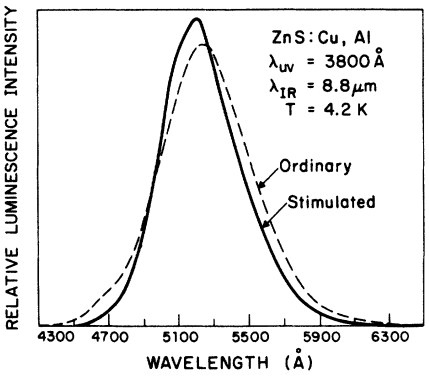

FIG. 4. Ordinary and stimulated luminescence spectra. Note blue shift of stimulated spectrum.

der conditions of steady ultraviolet excitation and exposure to repetitive pulses of infrared radiation. The dashed-line spectrum was taken with the boxcar integrator gate set slightly before the rise of the stimulated luminescence, and the solid-line spectrum was taken with the gate set at the peak of the stimulated luminescence and the dc luminescence component filtered out. The stimulated photoluminescence peak is slightly blue-shifted with respect to the ordinary photoluminescence peak. The 4700-Å shoulder in the ordinary luminescence spectrum is a second luminescence peak, which is not infrared stimulable and hence does not appear in the stimulated luminescence spectrum.

Photoexcitation spectra for both the stimulated and ordinary photoluminescence were also taken and found to be essentially identical. These were done with low resolution to obtain adequate amounts of excitation intensity. The spectra are similar to those reported by other workers, peaking at about 4000 Å for the ZnS:Cu, Al sample.

E. Dependence of stimulated luminescence on infrared and ultraviolet radiation intensity, and on temperature

All the data presented in this section were taken using the second experimental arrangement described in Sec. II A, which employed a chopped (4% duty cycle) 10.6-μm CO_2 laser as the infrared-radiation source. Figure 5 shows the effect on the luminescence of reducing the photoexcitation intensity with neutral-density filters while keeping the infrared-radiation intensity and temperature constant ($T = 5$ K). The ordinary luminescence intensity varies nearly linearly with photoexcitation intensity, as might be expected if nonradiative losses are small. The stimulated-luminescence transient-peak intensity varies approximately as the 0.63 power of the photoexcitation intensity. Thus the ratio of the stimulated to ordinary luminescence decreases with increasing photoexcitation intensity.

The effect on the stimulated luminescence of varying the infrared-radiation intensity while keeping the photoexcitation intensity and temperature constant is shown in Fig. 6. The stimulated-luminescence intensity first increases approximately as the 0.65 power of the infrared-radiation intensity and then passes through a maximum as the infrared-radiation intensity is increased further. The rise time for the stimulated luminescence is less than that of the pulse of infrared radiation for high-infrared-radiation intensity and increases with decreasing intensity to about 2 or 3 msec at the lowest infrared-radiation intensity used. It can be estimated (see Sec. V C) that this lowest intensity is comparable to that of the infrared diode used in obtaining the waveform of Fig. 1, which

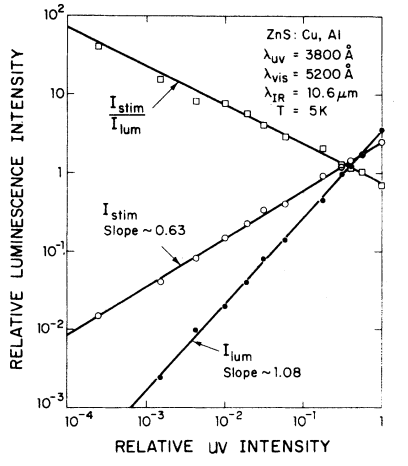

FIG. 5. Variation of ordinary (I_{lum}) and stimulated (I_{stim}) luminescence intensity with photoexcitation intensity. Note that ratio I_{stim}/I_{lum} decreases with increasing photoexcitation intensity.

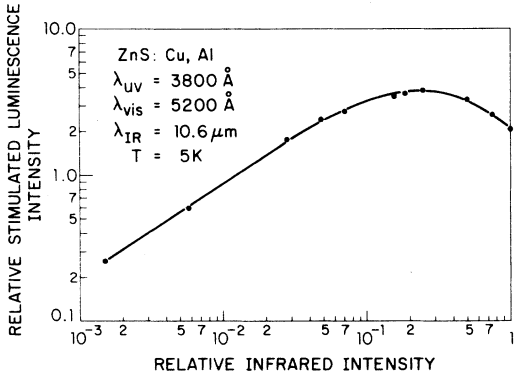

FIG. 6. Variation of stimulated luminescence intensity with infrared radiation intensity.

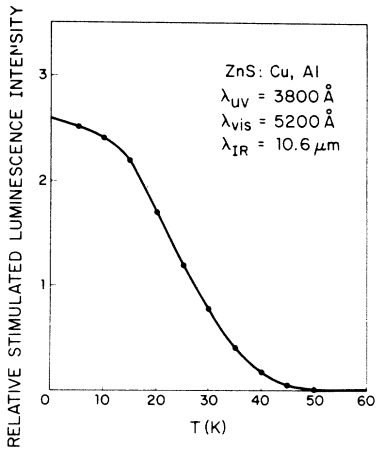

FIG. 7. Temperature dependence of stimulated luminescence intensity.

has a rise time of about 5 msec.

The change with temperature of the stimulated-luminescence intensity for fixed photoexcitation and infrared-radiation intensity is shown in Fig. 7. This result is similar to that reported by Riehl *et al.*[6]

III. RATE EQUATIONS

The model outlined qualitatively in Sec. I and illustrated in Fig. 8 can be formulated quantitatively by extending Dohler's recent treatment of the kinetics of donor-acceptor transitions.[7] This treatment proceeds by assigning to each donor two time-dependent probability functions. The first function is the probability $\rho(r, t)$ that the nearest unoccupied acceptor (acceptor with a hole) is a distance r away. For a statistical distribution of unoccupied acceptors of density n_{A0}, $\rho(r, t)$ is given by

$$\rho(r, t) = 4\pi n_{A^0}(t) r^2 \exp[-\tfrac{4}{3}\pi n_{A^0}(t) r^3], \quad (1)$$

and has the property that

$$\int_0^\infty \rho(r, t)\, dr = 1, \quad (2)$$

independent of $n_{A0}(t)$. As indicated, the time dependence of $\rho(r, t)$ enters through the possible time dependence of $n_{A0}(t)$. When $n_{A0}(t)$ is zero, $\rho(r, t)$ is also zero, and cases where this can occur must be handled with care, although there is seldom any real difficulty. The second function is the probability $Q(r, t)$ that a donor with its nearest unoccupied acceptor a distance r away is itself occupied. As usual, it is assumed that the transition probability $W(r)$ for direct radiative recombination between an electron on a donor and a hole on an acceptor a distance r away varies as

$$W(r) = W_0 e^{-r/r_0}, \quad (3)$$

where r_0 is half the donor Bohr radius a_0, or a number chosen to agree with experiment. The essential feature that makes Dohler's formulation fairly tractable is the assumption that the strong r dependence of $W(r)$ justifies neglecting the possibility of transitions between an occupied donor and any unoccupied acceptor other than the nearest one. For the purposes of the present paper, it is also necessary to make some specific assumptions about the nature of photoexcitation and trapping. In the experiments reported here, the photoexcitation energy was about 3.26 eV, which is less than the ZnS gap energy of about 3.65 eV. It is commonly believed that acceptors in ZnS are fairly deep (1–2 eV) and that photoexcitation at energies less than the gap energy lift electrons from occupied acceptor levels to the conduction band.[8] From the conduction band, trapping occurs with equal probability to any unoccupied donor. No distinction is made between electrons present in the conduction band due to photoexcitation or due to infrared-excited donor–to–conduction-band transitions.

With the preceding assumptions, the rate equations describing the model of Sec. I are

$$\frac{dM}{dt} = I_{uv} C n_{A^-} + B n_{D^0} I_{ir} - T n_{D^+} M, \quad (4a)$$

$$\frac{dn_{D^0}(r)}{dt} = -B n_{D^0}(r) I_{ir} + T n_{D^+}(r) M - n_{D^0}(r) W(r). \quad (4b)$$

In Eq. (4a), M, n_{D^+}, n_{D^0}, and n_{A^-} are, respectively, the numbers of conduction band electrons, empty donors, filled donors, and filled acceptors per unit volume. I_{uv} and I_{ir} are, respectively, the numbers of incident photoexcitation and infrared photons per unit time per unit area. C and B are the absorption cross sections of occupied acceptors and occupied donors, respectively, for photoexcitation and infrared photons. The I_{uv} and I_{ir} terms thus neglect the decrease in photoexcitation and infrared intensity through the sample thickness due to absorption. T is a trapping coefficient with units of volume per time. In Eq. (4b) $n_{D^0}(r)$ and

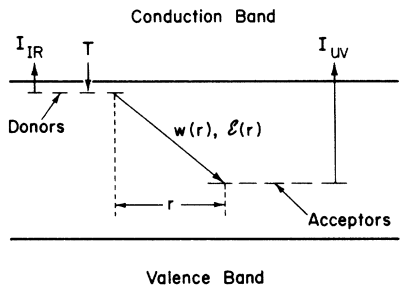

FIG. 8. Energy-level diagram illustrating stimulation model.

$n_{D^+}(r)$ are, respectively, the number of filled and empty donors with nearest unfilled acceptor a distance r away. These two quantities are related to ρ, Q, n_{D0}, n_{D^+} by the equations

$$n_{D0} = \int_0^\infty n_D \rho(r, t) Q(r, t)\, dr = \int_0^\infty n_{D0}(r)\, dr,$$
$$n_{D^+} = \int_0^\infty n_{D^+}(r)\, dr = n_D \int_0^\infty \rho(r, t)[1 - Q(r, t)]\, dr, \tag{5}$$

where n_D is the donor density. Charge conservation assures that the following relations are satisfied at any time t:

$$n_{A0} = n_A - n_D + M + n_{D0},$$
$$n_{A^-} = n_A - n_{A0} = n_{D^+} - M. \tag{6}$$

The rate equations obtained by inserting Eqs. (5) and (6) into Eqs. (4a) and (4b) are very tedious to solve, as discussed in Appendix B. A set of equations which is simpler, but nonetheless captures much of the essential behavior of the model, is obtained in the approximation that n_D, $M \ll n_A$. This inequality implies that $n_{A0} \approx n_A \approx$ const, so that ρ is time independent. Also implied is that $n_{A^-} \approx n_D$, so the photoexcitation term $I_{uv} C n_{A^-}$ in Eq. (4a) is set to a constant, $I_{uv} A$. The constant $A = n_D C$ has units of inverse length and is an absorption coefficient. With these approximations, Eqs. (4)–(6) may be combined to give the following normalized and dimensionless rate equations:

$$\frac{dm(\tau)}{d\tau} = J + I \int dr'\, \rho(r') Q(r', \tau) - m(\tau) \int dr'\, \rho(r')[1 - Q(r', \tau)],$$
$$\frac{dQ(r', \tau)}{d\tau} = IQ(r', \tau) + m(\tau)[1 - Q(r', \tau)] - w(r) Q(r', \tau). \tag{7}$$

Definitions of the various normalized quantities are given in Table I.

The approximation $n_D \ll n_A$, made in obtaining Eqs. (7), is not actually appropriate to ZnS. Efforts to dope ZnS nearly always yield highly resistive n-type material, which suggests that $n_D \gtrsim n_A$. In this case n_{A0} will be small in the absence of photoexcitation, and will tend to be time dependent. Thus the parameter $n_0 = \frac{4}{3}\pi r_0^3 n_{A0}$ defined in Table I must be regarded as an effective average quantity in applying Eqs. (7) to ZnS.

In terms of the normalized quantities, the total number of emitted photons per second per unit volume at time $t = \tau/(n_D T)$ is $(n_D^2 T) F(\tau)$, where $F(\tau)$ is defined by

$$F(\tau) = \int_0^\infty dr'\, \rho(r') Q(r', \tau)\, w(r') \equiv \int_0^\infty dr\, G(r'). \tag{8}$$

Similarly, the number of trapped electrons per unit volume at time $t = \tau/(n_D T)$ is $n_D q(\tau)$, where $q(\tau)$ is defined by

$$q(\tau) = \int_0^\infty dr'\, \rho(r') Q(r', \tau). \tag{9}$$

TABLE I. Definitions of normalized quantities appearing in Eqs. (7).

$J \equiv \frac{I_{uv} A}{n_D^2 T}$	$w_0 \equiv \frac{W_0}{n_D T}$
$I \equiv \frac{I_{ir} B}{n_D T}$	$m \equiv \frac{M}{n_D T}$
$w = \frac{W}{n_D T}$	$\tau \equiv (n_D T) t$
$n_0 \equiv \frac{4}{3}\pi n_{A0} r_0^3$	$r' = r/r_0$
$\rho(r') = 3 n_0 r'^2 e^{-n_0 r'^3}$	

IV. BASIC BEHAVIOR OF THE MODEL

Numerical solutions for the Eqs. (7) have been obtained for cases where I and J are changed abruptly from one value to another and the initial values of m and $Q(r)$ are given. Frequently, but not always, the initial values are taken to be the equilibrium values for fixed I and J. This procedure is adequate to simulate most of the experiments described in Sec. II. The method of finding the equilibrium values and the time dependence resulting from a change in I or J is described briefly in Appendix A. Figures 9–11 present the solutions obtained for various choices of $I(\tau)$ and $J(\tau)$ with $w_0 = 0.77 \times 10^{-5}$ and $n_0 = 0.45 \times 10^{-2}$. These choices simulate, respectively, the experimental situations leading to the data of Figs. 1–3. The values of I and J used are given in the figures. These values are much larger than appropriate to experiment, but they give behavior that is fast in τ time and therefore permit various possibilities to be explored with minimal computer time. These solutions illustrate the basic behavior of the model and show that it is in good qualitative agreement with the experimental results of Sec. II. Section V discusses the extent to which quantitative agreement with experiment can be obtained by varying the model parameters.

In the experimental situation of Fig. 1, the photoexcitation was constant and steady infrared radiation was abruptly turned on. This situation can be simulated in the model by taking J to be a constant and I to be a step function at $\tau = 0$, with $m(0)$ and $Q(r', 0)$ being their equilibrium values for the constant J and $I = 0$. Figure 9 shows the time evolution of m, q, F, and Q resulting from the abrupt turning-on of I. These curves illustrate the basic behavior of the model, as anticipated qualitatively in Sec. I B. The equilibrium trap population for constant J and zero I is given by the initial values of Q, which range from Q near 1.0 for large r' to 10^{-3} for small r'. The change from Q near 1.0 to Q very small always occurs over a

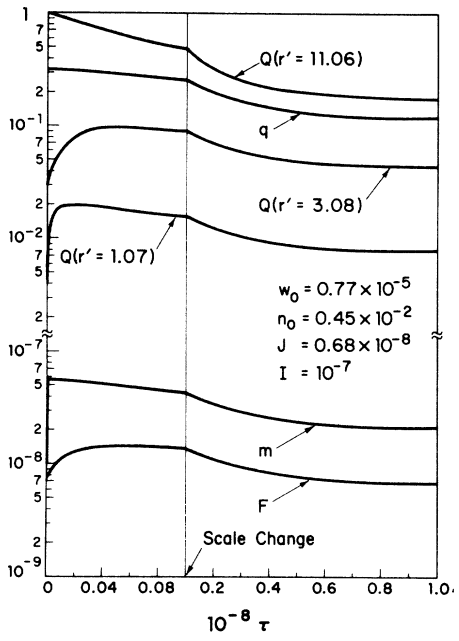

FIG. 9. τ dependence of m, q, F, and Q for three r' values, illustrating basic kinetics of model for steady photoexcitation and step-function infrared radiation. Note fast rise and slow fall of F.

narrow range of r', in this case between $r' = 3$ and $r' = 5$. This variation of Q with r' is, of course, the result of the exponential variation with r' of the transition probability $w(r')$. When I is turned on at $\tau = 0$, stored electrons are dispelled from the large-r' traps, through the conduction band and out the small r' traps via radiative recombination with holes. The large-r' Q decrease steadily to new lower values, and the small-r' Q rise quickly to peak values and then return slowly to new values slightly greater than their initial ones. F, which is proportional to the emitted light intensity [see Eq. (8)], follows the behavior of the small-r' Q and rises quickly to a peak and then falls slowly to its final value. In accordance with the conservation principle given in Appendix A [Eq. (A2)], the initial and final values of F are both equal to J. The fast rise and slow fall of F is qualitatively like the experimental behavior shown in Fig. 1. The stored charge q [see Eq. (9)], to which the infrared absorption induced by photoexcitation is proportional, follows the behavior of the large-r' Q and decreases steadily from its initial value to a new lower value. It is clear that the transient change in F is due to the decrease of q. Qualitatively, the slow steady change of q, with little change during the time when F peaks, is like the time dependence observed for the infrared absorption, as described in Sec. II C.

The large transient increase in Q for small r' results in a transient increase in the value of r' for which the integrand of Eq. (8) peaks, from about $r' = 4.8$ at $\tau = 0$ to about $r' = 3.2$ at the value of τ where F peaks. Since the emitted photon energy is larger for small-r' donor-acceptor pairs, this means that the luminescence is transiently blue shifted, as in the experimental result shown in Fig. 4. Using the energy formula $e^2/\kappa r$, and taking[7] $\kappa = 8$, $r_0 = 5$ Å (recall that $r' = r/r_0$ from Table I), the r' shift of Fig. 10 implies an energy shift of about 32 meV, or about 70 at 5200 Å. This is the order of magnitude of the experimental shift shown in Fig. 4.

The effect of abruptly returning I to zero at two

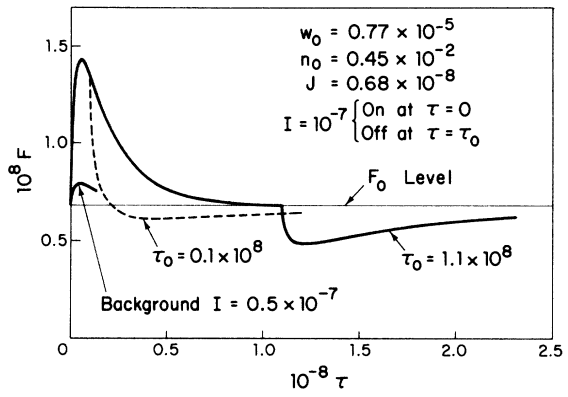

FIG. 10. Effect on F of returning I to 0 at two different τ's for the case shown in Fig. 9. Reduced initial transient change in F for case of Fig. 9, but with background I present, is also shown.

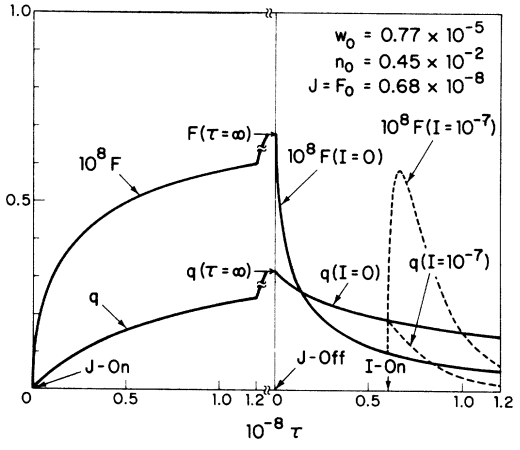

FIG. 11. Buildup and decay of F and q for step function J on and off. Dashed lines show effect of step function I applied during decay. Note that q responds to changes in J much more slowly than F. Parameter values are same as for case of Fig. 9.

different times is shown in Fig. 10. Computationally the curves are obtained by keeping J unchanged, and setting I to zero with initial values of m and Q taken as their values in Fig. 9 either at $\tau = 0.1 \times 10^8$ (the Fig. 9 scale interchange) or $\tau = 1.1 \times 10^8$, which is essentially infinity.

For the case where I is returned to zero before equilibrium is reached (dashed curve), F falls fairly quickly to a value somewhat lower than J, and then rises slowly back to J. This result should be compared with the data of Fig. 2, which show very similar rise-and-fall behavior, but does not show a dip below the initial value. It should be pointed out that the model calculation does not precisely simulate the experimental situation of Fig. 2, in that the calculation is for a single infrared pulse rather than a repetitive pulse series, and the disagreement may be related to this. If I is returned to zero after equilibrium is reached (solid curve), F falls fairly quickly to a minimum well below J, and then returns very slowly to J. This is exactly what is observed experimentally, as described in Sec. II C. Here, the model calculation does simulate the experimental situation.

Figure 10 also shows the initial transient change in F for I abruptly changed from 0.5×10^{-7} to 1.5×10^{-7} with initial values of m and Q the equilibrium m, Q, appropriate for the same steady J and $I = 0.5 \times 10^{-7}$. This simulates the presence of some fairly intense background infrared radiation such as might be found with a low-intensity but broadband thermal source. The transient change in F is considerably reduced from the no-background case, which is consistent with the experimental necessity of protecting the sample from unintentional exposure to infrared radiation, as mentioned in Sec. II A. This result may also provide a partial explanation for the temperature dependence of the stimulation effect, shown in Fig. 7, if the effect of increasing temperature is to free trapped electrons to the conduction band, thus simulating the presence of background infrared radiation. This explanation is incomplete, however, as discussed in Sec. VI.

For $I = 0$ and $J = 0$, the equilibrium values of m and $Q(r')$ are zero. If J is abruptly turned on at $\tau = 0$, and I remains 0, F and q change as shown in the left half of Fig. 11. F changes more quickly than Q because the small-r' Q change more rapidly than the large-r' Q. The conduction-band population m (not shown in the figure) jumps very quickly to about 70% of its final value at $\tau = 5.0$, and then moves very slowly to its final value. If J is set abruptly to zero, with initial values of m and Q taken as their equilibrium values for steady J and zero I, the behavior of F and q is as shown in the right half of Fig. 11. Again F changes more quickly than q because $Q(r')$ changes more quickly for small r' than large r'. The dashed lines in Fig. 11 show the effect on F and q of suddenly turning on I at $\tau = 0.6 \times 10^8$ past the time when J was set to zero. There is a large transient increase in F followed by a faster decay than for the $I = 0$ curve. It is clear that the dashed F curve will cross the solid one slightly beyond the boundary of the figure. The peak increase in F is about 75% of that for the constant-J case, even though F has decayed to about 15% of its constant-J value. The results in Fig. 11 are largely in accord with the experimental observations described in Sec. II C in connection with Fig. 3, even though the calculation does not exactly simulate the experimental situation in that, experimentally, J and I are repetitive pulses, and calculationally they are step functions. In particular, both the luminescence and the stored charge respond sluggishly to abrupt changes in photoexcitation, with the stored charge having, by far, the slower response.

V. EFFECT OF VARYING MODEL PARAMETERS AND NUMERICAL COMPARISON WITH EXPERIMENT

A. Variation of τ_m and $[F(\tau_m) - F(0)]$ with J, n_0, I, and w_0

The two experimental quantities most readily compared with the theory are the time required to reach the luminescence peak after applying infrared radiation, t_m, and the ratio of the peak change in luminescence to the initial value of luminescence. Therefore the variation of the theoretical quantities $[F(\tau_m) - F(0)]/F(0) \equiv \Delta F/J$ [see Eq. (A2)] and $\tau_m = (n_D T) t_m$ with the parameters of the theory is of interest.

Figures 12 and 13 show τ_m and ΔF as a function of J for various choices of I, n_0 and w_0. It can be seen in Fig. 12 that with increasing J, τ_m decreases. The slanted lines in Fig. 13 are lines of constant $\Delta F/J$. With increasing J, ΔF first in-

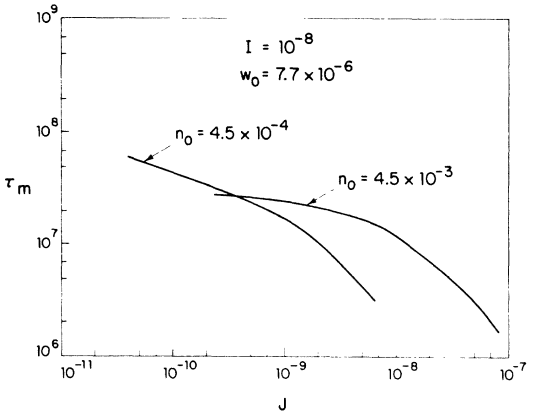

FIG. 12. Variation with J of τ_m for various values of n_0.

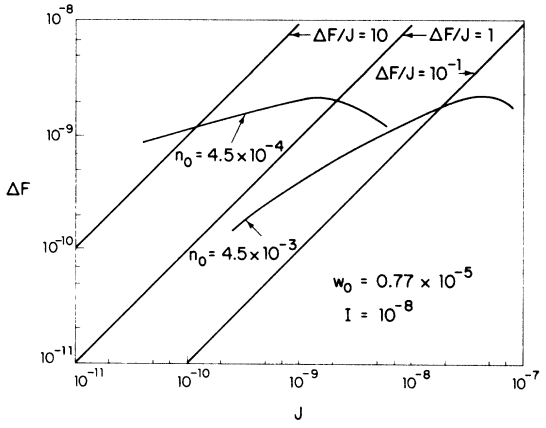

FIG. 13. Variation with J of ΔF for various values of n_0. Slanted lines show constant $\Delta F/J$. Note that $\Delta F/J$ decreases with increasing J.

creases and then passes through a maximum and decreases. The ratio $\Delta F/J$ steadily decreases with increasing J, as anticipated qualitatively in Sec. I B, and observed experimentally (see Fig. 5).

The effect of altering n_0 can also be seen in Figs. 12 and 13. Over most of the range of J, increasing n_0 decreases F. This is probably due to the decrease in stored charge with increasing n_0, brought about by a decreased average donor-acceptor spacing. It can be noted that the maximum in $\rho(r')$ occurs for $r' = (\frac{2}{3}n_0)^{1/3}$. There is some experimental evidence[13] that very heavy doping of ZnS phosphors greatly reduces long-wavelength infrared stimulation, which agrees with the theoretical result.

Figure 14 shows ΔF and τ_m as functions of I for particular choices of J, n_0, and w_0. These results are intuitively sensible, with an increase in I resulting in more stored charge being driven out faster. The experimental and dashed curves in Fig. 14 will be discussed below (Sec. V B).

The effect of varying w_0 has been studied the least. It is not readily varied experimentally, and fairly reliable values for W_0 are available in the literature. The results that have been obtained indicate that ΔF and τ_m are much less sensitive to w_0 than to the other three parameters discussed in this section.

B. Numerical comparison of theory and experiment

To try to make a numerical comparison of theory and experiment it is necessary to decide what values of I, J, n_0, and w_0 are appropriate for actual experimental conditions, and this not entirely straightforward. Values for I, J, and w_0 have been selected on a "best estimate" basis with no effort to choose values that yield agreement of theory and experiment. Values for I, J, and w_0 entail a choice for $n_D T$. Although the results of Appendix C show that the choice is fairly arbitrary, there is no reason not to try to be realistic. T can be estimated as the product of the thermal velocity v_t and the trapping cross section σ. Taking the temperature θ as 4 K and $m^* = 0.34 m_0$,[13] $v_t = (3k\theta/m^*)^{1/2} = 2.3\times10^7$ cm/sec. Estimating σ as intermediate between the geometrical value πa_0^2 ($a_0 \approx 10$ Å)[7,12] and the value allowing the donor's Coulomb force to overcome the electron's thermal energy suggests $\sigma \approx 4\times10^{-14}$ cm^2, so $T \simeq 10^{-6}$ cm^3/sec. Mass spectrograph analysis of the samples used suggests $n_D \approx 10^{18}$ cm^{-3}, giving $n_D T \approx 10^{12}$ sec^{-1}. W_0 has been experimentally found to be about 10^7 sec^{-1},[7,12] giving $w_0 = W_0/n_D T = 10^{-5}$. The infrared-radiation parameter is $I = I_{ir}B/n_D T$. From the work of Kukimoto *et al.*,[12] B is estimated to be 2.8×10^{15} cm^{-2} for $\lambda_{ir} \approx 9$–10 μm. It is believed that the 8.8-μm laser diode delivers about 100 μW to a sample area of 0.25 cm^2, which implies that $I_{ir} = 1.8\times10^{14}$ photons sec^{-1} cm^{-2}, so that $I \approx 5\times10^{-11}$ for the laser diode. The optical pump parameter is $J = I_{uv}A/n_D^2 T$. At 3800 Å, A was measured to be about 100 cm^{-1}, and I_{uv} was measured, using an Epply thermopile, to be 8×10^{14} photons sec^{-1} cm^{-2}. Thus J is estimated to be 8×10^{-14}.

The quantity n_0 is given by $\frac{4}{3}\pi r_0^3 n_{A0}$. As explained at the end of Sec. III, n_0 is at best an effective parameter for the application of Eqs. (7) to ZnS. It has been found that a value of $n_0 \approx 10^{-3}$, equivalent to taking $n_{A0} \approx 1.9\, n_D$, yields fair agreement of theory and experiment, using the values of I, J, and w_0 estimated above.

For the parameters just estimated, $n_0 = 10^{-3}$, $w_0 = 10^{-5}$, $J = 8\times10^{-14}$, and $I = 5\times10^{-11}$, it was found that τ_m was so large that an excessive amount of computer time would be required to find ΔF and

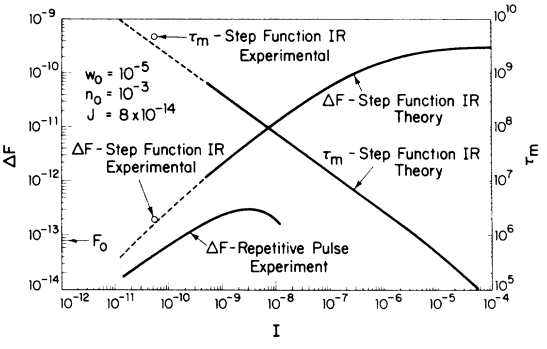

FIG. 14. Variation with I of ΔF and τ_m for parameter values estimated to correspond to experiment. Dashed lines show extrapolation to small I values. Open circles show experimental τ_m and ΔF for step-function infrared radiation, determined from data of Fig. 1. Also shown are experimental data of Fig. 6. See text for comments.

τ_m. Therefore ΔF and τ_m were found for a series of larger values of I, which could be done with a fairly small amount of computer time, and the results were extrapolated to small values of I, as shown by the dashed lines in Fig. 14. The extrapolation suggests that for the estimated experimental parameters the model gives $\Delta F/J \approx 1.9$ and $\tau_m \approx 3.5\times10^9$. This value of τ_m corresponds to a value of $\tau_m = \tau_m/n_D T = 3.5$ msec. Thus both $\Delta F/J$ and t_m are fairly close to the values obtained using the laser diode, as shown by the open circle points of Fig. 14, obtained from the data of Fig. 1.

It is also of interest to compare the curves of Fig. 14 with the data obtained using the CO_2 laser at 10.6 μm, shown in Fig. 6. The data of Fig. 6 were plotted in Fig. 14 using the information that the largest infrared intensity in Fig. 6 was about 100 mW/cm^2 and letting ΔF have the value that made $\Delta F/J$ for the theory the same as the ratio of stimulated to background luminescence intensity in the data. As can be seen, the agreement is only fair as to the slope of the curves where they are roughly linear and the maximum in the data is not given by the theory at all. The fact that the experimental curve lies below the theoretical one is not so disturbing in that the theoretical I is a single step function and the experimental I is a repetitive pulse train. Experiments with the laser diode (Sec. II C) showed that the stimulated signal is always smaller for repetitive pulses than for a step function, presumably because there is inadequate time between pulses for stored charge replenishment.

Figure 15 shows the model results for the variation of $\Delta F/J$ with J for $n_0 = 10^{-3}$, $w_0 = 10^{-5}$, $I = 5\times10^{-9}$, compared to the data of Fig. 5. The theoretical slope is in bad agreement with the measured one, possibly due to ignoring the dependence $n_A{}^0$ on time and photoexcitation intensity (see end of Sec. III).

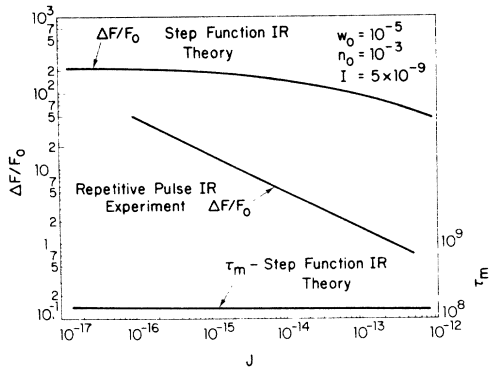

FIG. 15. Variation with J of $\Delta F/F$ ($\tau = 0$), theory, and data of Fig. 5. See text for comments.

To sum up, the model reproduces most of the qualitative effects in the data, and gives the right order-of-magnitude results for $\Delta F/J$ and τ_m, but it does badly on a detailed quantitative basis.

VI. DISCUSSION

The model presented in this paper is the first quantitative effort to explain the kinetic behavior of stimulated luminescence within the framework of the theory of donor-acceptor pair luminescence. This treatment is based on Dohler's work[7] and extends his work in two ways. First, Dohler did not consider the details of the photoexcitation and trapping processes, or formulate his treatment in terms of rate equations, as was necessary for the calculations described here. He considered the cases of luminescence with steady photoexcitation, decay of luminescence following steady photoexcitation, and decay of photoluminescence following a pulse of photoexcitation. Because they involve steady photoexcitation, the first two cases can be handled without rate equations and without considering the details of the photoexcitation and trapping processes. This is not true for the last case, where the photoexcitation does not last long enough to produce an equilibrium situation. Dohler assumed that immediately after a pulse of photoexcitation, $Q(r, 0) = Q_0 = \text{const}$. Given the assumptions about photoexcitation and trapping embodied in Eq. (7), the curves in the left half of Fig. 11 show that Dohler's assumption is not strictly valid, in that the various $Q(r)$ increase from 0 at different rates. The second extension of Dohler's work is, of course, the inclusion of a mechanism for infrared stimulation.

The author is aware of only one other quantitative treatment of such effects, by Matossi[14] in 1956. His efforts were directed at understanding experimental observations of dynamic infrared quenching of photoconductivity and luminescence in CdS. Matossi formulated and solved rate equations for a model consisting of three single energy levels, the conduction band, traps, and luminescence centers. Luminescence was assumed to arise from conduction-band–to–luminescence-center transitions, and all the traps were treated on an equal footing. The present theory differs from his principally in the additional conceptual input from the donor-acceptor pair luminescence model.

The understanding of many of the luminescence bands in ZnS has consisted of a gradual recognition of the necessity for the concepts of the donor-acceptor pair model. This evolution in thinking can be traced in a series of papers by various authors dating from the proposals of Prener and Williams[15] in 1956, and culminating in the more recent work of Shionoya and co-workers,[8–12] and of Riehl, Baur, and co-workers.[6] Thus, in con-

sidering their longer-wavelength–infrared-stimulation results, the discussion of Baur *et al.*[3–6] is very much in the context of the donor-acceptor pair model. But their description of the stimulation process differs from the model of this paper in that they were most reluctant to ascribe the effect of the infrared radiation to the production of donor-level–to–conduction-band transitions, despite the fact that this is the simplest assumption that can be made, and the existence of experimental evidence by Kukimato *et al.*[12] that such an infrared absorption process does occur. As best the author can understand from reading the discussions of Baur *et al.*, this reluctance stemmed from the belief that the assumption of donor–to–conduction-band transitions also entailed the conclusion that the stimulated luminescence was due to conduction-band–to–acceptor transitions, which would be inconsistent with the experimental properties of the luminescence. This difficulty is removed in the present model by the simple assertion that the electrons promoted to the conduction band are promptly retrapped. This assertion is almost demanded if it is assumed that photoexcitation consisting of acceptor–to–conduction-band transitions results in donor-acceptor pair luminescence. It would be very desirable to have direct experimental evidence on whether the infrared radiation promotes electrons to the conduction band. To that end attempts were made to observe the effect of the infrared radiation on the sample conductivity. These attempts failed due to difficulty in making electrical contact to the sample below 77 K, as mentioned in Sec. II A. However, Becker and Risgin[16] have observed infrared-induced photoconductivity in self-activated ZnS using infrared radiation with wavelengths as long as 5 μm, for which infrared stimulability is observed at temperatures of 77 K and above. Thus there is indirect evidence that long-wavelength infrared does promote electrons into the conduction band.

As pointed out in Sec. V, the model presented here is in good qualitative accord with the experimental kinetic data except in predicting that the stimulated luminescence saturates with increasing infrared intensity, rather than passing through a maximum, as observed. Additionally, the model is only partially successful on a quantitative basis.

There are several aspects of the experimental results that the model does not purport to explain, especially the infrared wavelength dependence and temperature dependence of the stimulated luminescence. Within the context of the model, the simplest explanation of the loss of stimulation with increased temperature is that increasing the temperature frees electrons from traps into the conduction band, simulating the presence of background infrared radiation. This possibility has been discussed by Baur *et al.* But with this explanation, it is difficult to understand why there continues to be infrared absorption induced by photoexcitation at temperatures well above those where stimulation is quenched, as reported by Kukimoto *et al.*,[12] and also observed in the samples used here.

The infrared wavelength dependence, within the context of the model, would most simply be attributed to the wavelength dependence of the infrared absorption induced by photoexcitation. Unfortunately, the infrared stimulation spectra reported by Baur *et al.*[5] are rather structured, while the induced-infrared-absorption spectra reported by Kukimoto *et al.*[12] are quite smooth, even though they occur in nearly the same wavelength range. Such comparisons should be made, however, between spectra taken on the same sample, since it is known that the impurity content of ZnS is exceedingly difficult to control. Also, there may be other sources of stimulation-spectra structure that are not accounted for in the present model. For example, the details of the transport process have been ignored. These may depend on the conduction-band state that is reached by an electron after infrared absorption, or may be complicated by the effects of a high-impurity density, as discussed, for example, by Redfield and Wittke.[17]

To summarize, the theoretical model of this paper describes fairly well most of the kinetic behavior of the long-wavelength infrared-stimulated luminescence at low temperatures. But there remain difficulties in understanding other aspects of the stimulation process. These aspects probably relate to the detailed quantum structure of the impurity states involved, and a good understanding may not result until optical-quality crystals with well-controlled impurity content become readily available.

ACKNOWLEDGMENTS

It is a pleasure to acknowledge a number of people who made essential contributions to this work: G. J. Iseler for critical discussions, advice, and encouragement; H. J. Zeiger for critical discussions and help in formulating and solving the kinetic equations; J. C. Mavroides for critical discussions and encouragement; H. R. Fetterman for assistance with the CO_2 laser; A. R. Calawa for providing a PbSnTe diode laser; S. N. Landon for programming the extensive computer computations; and L. G. B. Yee for creative technical assistance in the course of the experiments.

APPENDIX A: SOLUTION OF EQS. (7) AND CONSERVATION RELATION

Solutions to Eqs. (7) have been obtained for the case of I and J constant and initial values of m and

Q that are not the steady-state solutions appropriate to the values of I and J.

The steady-state (equilibrium) solutions of Eq. (7), obtained by setting $dm/d\tau = dQ/d\tau = 0$, are given implicitly by the two relations

$$m = \frac{J + I\int d\nu'\, \rho(\nu')Q(\nu')}{\int d\nu'\, \rho(\nu')[1 - Q(\nu')]},$$
$$Q(\nu') = \frac{1}{1 + [I + w(\nu')]/m}. \tag{A1}$$

The solutions of these equations are found by a self-consistent iterative procedure in which a trial m is assumed, Q is calculated, and m is then calculated with this Q and compared to the original trial value.

Equations (A1) can be used to find a conservation relation. By multiplying out the Q equation, eliminating m in it with the m equation, and performing $\int d\nu' \rho(\nu')$ on the result, it is found that for steady state

$$\int d\nu'\, \rho(\nu')Q(\nu')w(\nu') = J = m - (m + I) \times \int d\nu'\, \rho(\nu')Q(\nu'). \tag{A2}$$

The first equality reflects the fact that in this model there is no loss, so the total steady-state luminescence intensity must equal the pump intensity. The first equality also implies that the steady-state luminescence is independent of whether I is zero or not, so that the infrared stimulation of luminescence is transient.

The complexity of Eqs. (7) is pointed out by their mathematical characterization as an infinite nonlinear system of first-order ordinary differential equations with nonconstant coefficients. In the present treatment the coefficients are made constant by treating I and J as step functions, and the system is rendered finite by computing integrals over ν' by the method of Gaussian quadratures. Thereby the values of the integrand at only 16 values of ν' were required, so that the time evolution of only 16 Q's need be traced. The accuracy of the ν' integration could be verified by insisting that the steady-state conservation relation Eq. (A2) was satisfied. It was found that the proper upper-limit cutoff on the ν' integrals was sensitive to the value of n_0.

Initially an attempt was made to solve Eqs. (7) by straightforward point-by-point iteration using the first two terms of a Taylor series at each point. But it was found that the balance of terms in the $dm/d\tau$ equation was so delicate that very short time increments were required to keep the solution from diverging. These increments were much shorter than were required by the $dQ/d\tau$ equation and an immense amount of computer time was consumed without effecting much change in Q. This problem was avoided as follows. Assuming the τ dependence of Q is known, the exact formal solution of the $dm/d\tau$ equation can easily be written down and manipulated to express $m(\tau)$ in terms of $m(\tau - \Delta\tau)$ and integrals of functions involving $Q(\tau)$ in the intervals from $\tau - \Delta\tau$ to τ:

$$m(\tau) = \exp\left(-\int_{\tau-\Delta\tau}^{\tau} u(\tau')d\tau'\right) m(\tau - \Delta\tau) + \int_{\tau-\Delta\tau}^{\tau} d\tau' v(\tau') \exp\left(-\int_{\tau'}^{\tau} u(\tau'')d\tau''\right),$$

where

$$u(\tau) = J + I\int d\nu'\, \rho(\nu')Q(\nu', \tau),$$
$$v(\tau) = \int_0^\infty d\nu'\, \rho(\nu')[1 - Q(\nu', \tau)]. \tag{A3}$$

Q is extrapolated linearly between $\tau - \Delta\tau$ and τ by assuming

$$Q(\tau') = Q(\tau - \Delta\tau) + \left.\frac{dQ}{d\tau'}\right|_{(\tau-\Delta\tau)} [\tau' - (\tau - \Delta\tau)] \tag{A4}$$

for $\tau - \Delta\tau \leq \tau' \leq \tau$. Thus if m and Q are known at $\tau - \Delta\tau$, then Q is known approximately over the interval from $\tau - \Delta\tau$ to τ and m at τ can then be found. For example, the process might begin at $\tau = 0$ with the m and Q obtained from Eq. (A1) with $I = 0$ and continue until the m and Q obtained from Eq. (A1) with $I \neq 0$ are reached. The fact that the solutions do indeed go to the m and Q values computed from Eq. (A1) provides some confidence in the method. It was found that the largest possible step size $\Delta\tau$ is roughly $1/w_0$. For conservation of computer time, the computation may be carried only to τ_m sometimes. As the computation is carried out, quantities like F and q are also computed. Other combinations of step-function changes in I and J, as described in Sec. IV, can be handled within this framework.

APPENDIX B: IMPROVED TREATMENT OF ACCEPTORS

The rate equations obtained by inserting Eqs. (5) and (6) into Eqs. (4) and normalizing are

$$\frac{dm}{d\tau} = J[1 - \int d\nu' \rho(\nu', \tau)Q(\nu', \tau)] + I\int d\nu'\, \rho(\nu', \tau) \times Q(\nu', \tau) - m\left\{\left[1 - \int d\nu'\, \rho(\nu', \tau)\right] + J\right\},$$
$$\frac{d[\rho(\nu', \tau)Q(\nu', \tau)]}{d\tau} = [\rho(\nu', \tau) - \rho(\nu', \tau)Q(\nu', \tau)] - I\rho(\nu', \tau)Q(\nu', \tau) - W(\nu')\rho(\nu', \tau)Q(\nu', \tau), \tag{B1}$$

where the normalized quantities are as defined in Table I except for

$$J = I_{uv}C/n_D T,$$
$$n = \tfrac{4}{3}\pi r_0^3 n_D[(n_A/n_D) - 1 + m + \int d\nu'\, \rho(\nu', \tau)Q(\nu', \tau)],$$
$$\rho(\nu', \tau) = 3n(\tau)\nu'^2 e^{-n(\tau)\nu'^3}. \tag{B2}$$

Thus ρ is time dependent, being a function of $n(\tau)$, which is a functional of ρQ. It is therefore necessary to let m and ρQ be the independent variables

rather than m and Q, as in the case discussed in the text and in Appendix A. For the case where I and J are constant and the initial values of m and ρQ are not the steady-state values, Eqs. (B1) can be solved according to the same basic program as outlined in Appendix A for Eqs. (7). Given initial values of m and ρQ, then $\int dr'\,\rho(r',0)Q(r',0)$, n, and ρ can be found. The equation for $d(\rho Q)/d\tau$ can then be evaluated at $\tau=0$, and ρQ can be linearly extrapolated to its value at $\Delta\tau$. The exact formal solution of the $dm/d\tau$ equation can then be manipulated to give $m(\Delta\tau)$ in terms of $m(0)$ and integrals involving ρQ between 0 and $\Delta\tau$. Repetition of this process generates the solution.

Although the method of solving Eqs. (B1) is conceptually the same as for Eqs. (7), there is a difference in computational complexity, because it is necessary to reevaluate ρ at each new step in an iterative process. For example, the equations equivalent to Eqs. (A1) are

$$m=\frac{J[1-\int dr'\rho(r')Q(r')]+I\int dr'\,\rho(r')Q(r')}{1-\int dr'\,\rho(r')Q(r')+J},$$
$$\rho(r')Q(r')=\frac{\rho(r')}{1+\{[I+w(r')/m]\}} \tag{B3}$$

The solution proceeds iteratively by guessing a value for $\int dr'\,\rho(r')Q(r')$ and then computing m. Next ρ and ρQ can be found, and then the value of $\int dr'\,\rho(r')Q(r')$ is computed and compared to the original guess. As mentioned in Appendix A, the choice of limits in the integrations is quite sensitive to the shape of ρ, which is governed by the value of n. Since n is changing with each step of any of the iteration processes, it may be necessary to adjust the integral limits at each step. These various difficulties mitigated against an extensive study of the solutions of Eqs. (B1), although the results would be interesting and the solutions not impossible to obtain.

APPENDIX C: SCALING OF RATE EQUATIONS WITH $n_D T$

Equations (7) have an approximate scaling property that is important. The effect of changing $n_D T$ to $n_D T/\xi$ is, from the definitions in Table I, to multiply w, I, and J by ξ. If w, I, and J in Eqs. (7) are replaced by ξw, ξI, and ξJ, it is found that the equations can be rewritten in terms of $m'=m/\xi$ and $\tau'=\tau/\xi$ as

$$\frac{dm'}{d\tau'}=(1/\xi)\left\{J+I\int dr'\,\rho(r')Q(r')-m'\right.$$
$$\left.\times\int dr'\,\rho(r')[1-Q(r')]\right\}, \tag{C1}$$
$$\frac{dQ}{d\tau'}=-IQ+m'[1-Q]-wQ.$$

These equations differ from the original ones ($\xi=1$) only in the over-all factor of $1/\xi$ in the $dm'/d\tau'$ equation. Since the equilibrium values of m' and Q are found by setting Eqs. (7) to zero, as discussed in Appendix A, these equilibrium values will be the same as for m and Q when $\xi=1$. Further, it is found to be numerically true that for all the cases studied $dm'/d\tau'$ is so small that $m'(\tau')$ is very nearly given by setting the bracket of the $dm'/d\tau'$ equation to zero, so that the $1/\xi$ factor is unimportant. Thus the quantities $m'(\tau')$ and $Q(\tau')$ have the same values at $\tau'=\xi\tau$, for $\xi\neq1$, as did the quantities $m(\tau)$ and $Q(\tau)$ at time τ, for $\xi=1$.

The approximate scaling results imply that the two quantities most readily compared with experiment, $\Delta F/J$ and t_m (see Sec. V A), do not depend on $n_D T$ in this model. Both ΔF and J are multiplied by ξ when $n_D T$ is divided by ξ, since both are proportional to w, and hence their ratio is unchanged. τ_m is divided by ξ because the maximum in ΔF occurs when $\tau'=\xi\tau$ has the value of τ_m for $\xi=1$, and since t_m and τ_m are related by $t_m=\tau_m/n_D T$, t_m is also unaffected by dividing $n_D T$ by ξ.

---

†Work sponsored by the U. S. Air Force.

*Present address: Xerox Palo Alto Research Center, Palo Alto, Calif. 94304.

[1]Abstracts from the Session on Infrared-Sensitive Phosphors, Proceedings of the Winter Meeting of the Optical Society of America, March 1946 [J. Opt. Soc. Am. 36, 351 (1946)].

[2]D. E. Mason, Rev. Mod. Phys. 37, 743 (1965).

[3]G. Baur, J. Knobloch, N. Riehl, and P. Thoma, Z. Naturforsch A 21, 851 (1966).

[4] G. Baur, J. Knobloch, N. Riehl, and P. Thoma, in International Conference on Luminescence, Budapest, 1966 (unpublished).

[5]G. Baur, N. Riehl, and P. Thoma, Z. Phys. 206, 229 (1967).

[6]N. Riehl, J. Lumin. 1, 2, 1 (1970).

[7]G. H. Dohler, Phys. Status Solidi B 45, 705 (1971).

[8]A. Suzuki and S. Shionoya, J. Phys. Soc. Jap. 31, 1455 (1971).

[9]A. Suzuki and S. Shionoya, J. Phys. Soc. Jap. 31, 1462 (1971).

[10]K. Era, S. Shionoya, and Y. Washizawa, J. Phys. Chem. Solids 29, 1827 (1968).

[11]K. Era, S. Shionoya, Y. Washizawa, and H. Ohmatsu, J. Phys. Chem. Solids 29, 1843 (1968).

[12]H. Kukimoto, S. Shionoya, T. Koda, and R. Hioki, J. Phys. Chem. Solids 29, 935 (1967).

[13]G. W. Iseler (private communication).

[14]F. Matossi, J. Electrochem. Soc. 103, 662 (1956).

[15]J. S. Prener and F. E. Williams, Phys. Rev. 101, 1427 (1956).

[16]A. G. Becker and O. Risgin, in *Proceedings of the Third International Conference on Photoconductivity*, edited by E. M. Pell (Pergamon, New York, 1971), p. 117.

[17]D. Redfield and J. P. Wittke, Ref. 16, p. 29.

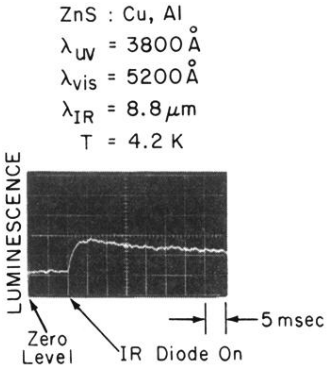

FIG. 1. Photograph of oscilloscope trace of photomultiplier current, showing transient change in steady photoluminescence due to step-function infrared radiation.